Quantifying Atomic Volume, Partial Charge, and Electronegativity in Condensed Phases

THE JOURNAL OF PHYSICAL CHEMISTRY C
A JOURNAL OF THE AMERICAN CHEMICAL SOCIETY

pubs.acs.org/JPCC

Article

Quantifying Atomic Volume, Partial Charge, and Electronegativity in Condensed Phases

Stefano Racioppi, Per Hyldgaard, and Martin Rahm*

Cite This: J. Phys. Chem. C 2024, 128, 4009−4017

Read Online

ACCESS | Metrics & More | Article Recommendations | Supporting Information

ABSTRACT: The predictive and explanatory roles of atomic properties such as size, charge, and electronegativity are closely linked to their definitions. However, establishing suitable definitions becomes increasingly challenging when examining atoms within materials. This study presents a quantum-mechanical framework for the quantitative assessment of these atomic properties in crystalline structures. Our approach utilizes Kohn−Sham density functional theory to approximate the electron energy density. We then employ a quantum chemical topological analysis of this density to derive atomic properties. The average electron energy density is conceptually powerful because it can be interpreted as a product of the electron density and the average energy of occupied molecular orbitals (MOs). Our method therefore bridges descriptive and predictive theories of electronic structure, including the quantum theory of atoms in molecules and MO theory. The applicability of our methodology is demonstrated across various materials, including metals, ionic salts, semiconductors, and a hydrogen-bonded molecular crystal. This work provides insights into electronegativity inversion during bond formation. It also highlights the complementary roles of partial charge and electronegativity in electronic structure analysis, with one indicating spatial electron accumulation or depletion and the other reflecting average electron binding. Experimental ground state electronegativities of H^-, Li^+, C^+, N^-, O^-, F^-, K^+, and Ga^+ are provided to support our discussion.

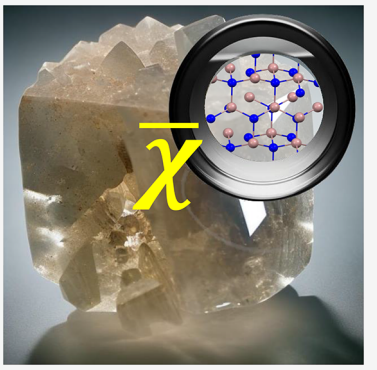

INTRODUCTION

In this work, we outline a computational method for quantifying electronegativity, partial charge, and volume of atoms and ions inside crystalline materials. Our approach follows previous efforts where these same conceptually important properties are calculated for atoms inside molecules.[1]

The quantification of concepts such as electronegativity, size, and the disposition of electrons inside materials is fraught by difficult choices of how to do so.[2−6] However, quantify them we wish because they are often helpful for rationalizing aspects of observable chemistry. Challenges arise because there exists no one unique definition to either property but a plethora of methods, scales, and principles. We note that relatively few approaches are computationally practical and applicable to extended (e.g., solid state) systems, as opposed to molecules. Among these approaches, the quantum theory of atoms in molecules (QTAIM) by Bader, in primis, gave to theoreticians and experimentalists a tool to calculate, among several other properties, atomic charges, and atomic volumes inside of materials from the electron density.[7] Hirshfeld, instead, proposed an alternative way to decompose real space into atomic fragments based on the weighted contribution of each atoms to the total electron density of a system.[8] Together with other types of geometrical partitions, like the Voronoi cells,[9] those methods became useful and efficient ways to compute atomic charges in periodic systems.

Electron density and interatomic distances are, however, only part of the criteria that can be used to partition and analyze materials. Orbital projection-based methods,[10] for example, use localized basis sets to evaluate Mulliken- and Löwdin-type charges in materials. Batsanov[11−14] even showed that thermochemical and spectroscopical experimental data can be used to evaluate electronegativities and charges of metal atoms in crystalline systems. Following the same general idea, several different researchers have combined effective charges with covalent or ionic radii in different semiempirical estimates of the electronegativity of atoms.[15−18] In this context, Pendás and co-workers,[19] following the works by Boyd et al.,[20,21] have shown that a correlation exists between QTAIM-determined ionic radii in alkali halides crystals and tabulated Pauling electronegativity of atoms. Komorowski has formulated electronegativity in terms of a bonding potential term that can be approximated in different ways for ionic and covalent solids.[22,23] Van Genechten and co-workers[24] evaluated the average electronegativity of atoms inside crystals by calculating

Received: November 21, 2023
Revised: January 31, 2024
Accepted: February 2, 2024
Published: February 23, 2024

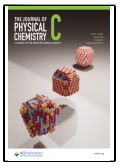

the corrective terms for the Mortier−Gosh−Shankar effective electronegativity[25] in solid-state systems with ab initio methods. An alternative route of atomic partitioning is the one explored by Tachibana, who used energy densities, and particularly, the kinetic energy density to study chemical reactions and shapes of atoms in the real space.[26]

Central to our approach for quantifying atomic volume, charge, and electronegativity in molecules is a topological analysis of the electron energy density, $X(\boldsymbol{r})$. The electron energy density is a product of the electron density $\rho(\boldsymbol{r})$ and a field representing the average electron potential, which we refer to as the average electron energy, $\overline{\chi}(\boldsymbol{r})$,

$$\mathrm{X}(\boldsymbol{r}) = \overline{\chi}(\boldsymbol{r})\rho(\boldsymbol{r}) \tag{1}$$

Equation 1 is conceptually appealing because it represents a union of sorts between two historically disparate frameworks for analyzing electronic structure. On the one hand, the direct topological partitioning of the electron density through the QTAIM,[7] and, on the other hand, molecular orbital (MO) theory.[27−29] The latter connection can be made because the average electron energy $\overline{\chi}$ can be approximated as an average energy of occupied orbitals, the electronic eigenvalues of a 1−determinant wave function

$$\overline{\chi} \approx -\sum_{i=1}^{n_{\mathrm{occ}}} \frac{\varepsilon_i}{N} \tag{2}$$

where n_{occ} is the number of occupied spin orbitals, ε_i the eigenvalue associated with the ith spin orbital, and N is the total number of electrons. It is the quantity $\overline{\chi}$—when averaging only over valence electrons—that some of us and others have linked to the central concept of electronegativity[30,31] and used productively to make predictions on reactivity,[32,33] chemical bonding,[1,34,35] and high-pressure phenomena.[36]

The average electron energy $\overline{\chi}$ can be evaluated at varying levels of theory, at different computational costs.[34,37−39] One computationally attractive approximation to $\overline{\chi}$ within density functional theory (DFT), which we will extend upon herein, is to average eigenvalues of occupied Kohn−Sham (KS) orbitals. In our past work on molecules,[1] we have relied on such a KS-DFT approximation to $\overline{\chi}$ resolved in three dimensions,

$$\overline{\chi}(\boldsymbol{r}) \approx -\frac{\sum_i \varepsilon_i \rho_i(\boldsymbol{r})}{\rho(\boldsymbol{r})} \tag{3}$$

where $\rho_i(\boldsymbol{r})$ is a KS orbital density. The spatially resolved average electron energy $\overline{\chi}(\boldsymbol{r})$ described by eq 3 has also been extensively studied by Politzer, Murray, and co-workers (who, unlike us, refer to it as the local ionization energy).[37,40,41] Their work, which mostly focuses on the analysis of $\overline{\chi}(\boldsymbol{r})$ on molecular surfaces, usually defined by a 0.001 e·bohr^{-3} contours, have led to successful predictions of molecular reactivity and properties like Hammett constants,[42] reactivity,[43−46] pK_a,[47] atomic polarizability and volume,[48] local polarity,[49] and local electronegativity.[37,40,47,50,51] Alternative temperature-dependent expressions of the orbital-based approximation to $\overline{\chi}(\boldsymbol{r})$ in eq 3 have been studied by Bulat et al.[41] and Ayers et al.[52] Whereas we stay with a KS-approximation of $\overline{\chi}(\boldsymbol{r})$ in this work, the calculation of this potential can, in principle, be made at any level of accuracy. We refer the reader to ref 39 for a detailed review on possible approaches to evaluate $\overline{\chi}$ and $\overline{\chi}(\boldsymbol{r})$, and we will return in future work to describe and apply such more general approaches.

The average electron energy $\overline{\chi}(\boldsymbol{r})$ does not lend itself to conventional (QTAIM-like) quantum chemical topological analysis.[41] One reason for the latter is that the topology of $\overline{\chi}(\boldsymbol{r})$ does not have critical points (maxima or minima) at nuclear positions. It is also not possible to meaningfully integrate finite values from $\overline{\chi}(\boldsymbol{r})$ and associate them with a region of space. To see why, it suffices to consider an isolated molecule for which $\lim_{r\to\infty} \overline{\chi}(\boldsymbol{r}) = \varepsilon_{\mathrm{HOMO}}$, where $\varepsilon_{\mathrm{HOMO}}$ is the energy of the highest (and most diffuse) occupied MO.[41] In other words, eq 3 has a divergent integral.

In our past work,[1] we instead pursued topological partitioning of the electron energy density, $X(\boldsymbol{r})$ (cf., eq 1). The topological features of $X(\boldsymbol{r})$ resemble those of the electron density—although effectively scaled by the value of the local electronegativity, $\overline{\chi}(\boldsymbol{r})$—with sharp cusps at nuclear coordinates and with the function decaying to zero at large distances from the nuclei. Our initial study relied on an orbital averaging approach (viz. eq 3) to compute $X(\boldsymbol{r})$ in molecules, we here take on the challenge of extending our approach to crystals.

THEORETICAL METHODS

Whereas eq 3 is straightforwardly applicable to molecules, its direct application to extended systems is not practical. To enable an extension of our methodology to crystals, we first express the KS approximation to the electron energy X in terms of energy functionals,[39,53]

$$\begin{aligned}\mathrm{X} &\approx -\sum_i \varepsilon_i n_i \\ &= -\left(T_{\mathrm{KS}}[\rho] + E_{\mathrm{Ne}}[\rho] + \int \upsilon_{\mathrm{xc}}(\boldsymbol{r})\rho(\boldsymbol{r})\mathrm{d}\boldsymbol{r} + 2J[\rho]\right)\end{aligned} \tag{4}$$

where n_i is the occupation number of the ith KS spin orbital, $T_{\mathrm{KS}}[\rho]$ is the kinetic energy of the noninteracting (KS) system, $E_{\mathrm{Ne}}[\rho]$ is the electron−nuclear attraction, $\upsilon_{\mathrm{xc}}(\boldsymbol{r})$ is the exchange-correlation potential, and $J[\rho]$ is the Hartree or mean-field electron repulsion energy,

$$J[\rho] = \frac{1}{2}\iint_{r,r_2} \frac{\rho(\boldsymbol{r})\rho(\boldsymbol{r}_2)}{|\boldsymbol{r}-\boldsymbol{r}_2|}\mathrm{d}\boldsymbol{r}\mathrm{d}\boldsymbol{r}_2 \tag{5}$$

We emphasize that eq 4 is an approximation and refer the interested reader to reference 53 for a detailed discussion on its origins and to ref 39 for a derivation of a formally exact expression.

To study $X(\boldsymbol{r})$, the spatial variation of all terms in eq 4 is needed. The kinetic energy density is not uniquely defined yet represents a crucial choice of our analysis. There exists several approximations to $T_{\mathrm{KS}}(\boldsymbol{r})$ expressed in terms of the total electron density $\rho(\boldsymbol{r})$ only.[37,52,54,55] We rely on a formulation of the kinetic energy density that directly derives from the application of the kinetic energy operator onto the first-order density matrix.[56] This kinetic energy density is expressed in terms of orbital densities $\rho_i(\boldsymbol{r})$, their gradients $\nabla\rho_i(\boldsymbol{r})$, and the Laplacian of total electron density $\nabla^2\rho(\boldsymbol{r})$:

$$T_{\mathrm{KS}}(\boldsymbol{r}) = \frac{1}{8}\sum_i \frac{\nabla\rho_i(\boldsymbol{r})\cdot\nabla\rho_i(\boldsymbol{r})}{\rho_i(\boldsymbol{r})} - \frac{1}{4}\nabla^2\rho(\boldsymbol{r}) \tag{6}$$

Note how, with this definition, the first term on the right-hand side of eq 6 integrates to the KS kinetic energy of the systems, while the Laplacian part, which allows local regions of space to have negative energy densities, integrates to zero.[56]

https://doi.org/10.1021/acs.jpcc.3c07677
J. Phys. Chem. C 2024, 128, 4009−4017

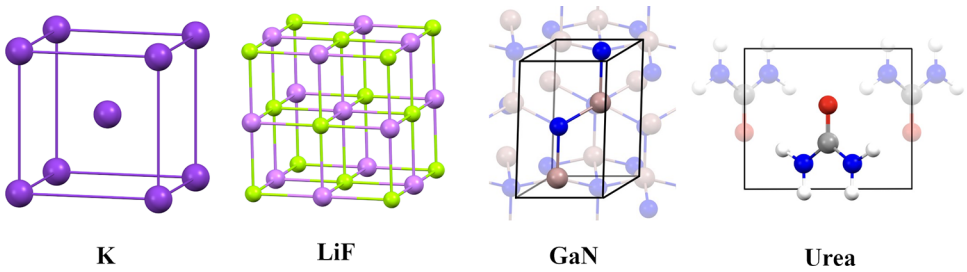

Figure 1. A test set of materials. Conventional unit cells of potassium (K, BCC), lithium fluoride (LiF, FCC), gallium nitride (GaN, wurtzite $P6_3mc$), and urea ($CO(NH_2)_2$, tetragonal $P\bar{4}2_1m$).

While there exists several (in principle infinite) other definitions for the kinetic energy density,[37,55,57,58] our choice of eq 6 can be motivated in different ways. First, we argue (like Bader before us[56]) that the "Schrödinger" or "Hamiltonian" form is the more natural choice. Second, this form is required to align our method with prior productive work on the use of the average electron (binding) energy to predict chemical reactivity, e.g., by Politzer and others.[37,41,44,47,49] Equation 6 provides the identical electron energy density $X(\boldsymbol{r})$ as eq 3, which have been used previously for molecules (see also Figure S1). Third, contrary to other tested choices for defining the kinetic energy density, the form of eq 6 results in workable topologies and atom-centered basins, which we will return to describe.

The remaining energy terms of eq 4 are more straightforward to translate into three dimensions. The electron nuclear attraction varies in space as

$$E_{\mathrm{Ne}}(\boldsymbol{r}) = \upsilon(\boldsymbol{r})\rho(\boldsymbol{r})\mathrm{d}\boldsymbol{r} \tag{7}$$

where $\upsilon(\boldsymbol{r})$ is the field generated by the presence of the nuclei that acts on the total electron density. The exchange-correlation potential $\upsilon_{\mathrm{xc}}(\boldsymbol{r})$ can take many different forms in DFT. In this work, we rely on the now classical Perdew–Burke–Ernzerhof (PBE) approximation.[59,60] Finally, the spatial resolution of the electron repulsion energy $J[\rho](\boldsymbol{r})$ is equal to twice the expression in eq 5 without the integration over d$\boldsymbol{r}$:

$$J[\rho](\boldsymbol{r}) = \int \frac{\rho(\boldsymbol{r})\rho(\boldsymbol{r}_2)}{|\boldsymbol{r} - \boldsymbol{r}_2|}\mathrm{d}\boldsymbol{r}_2 \tag{8}$$

The three potential energies, which describe all attractive and repulsive interactions, are by convention often recast in terms of the effective potential, $\upsilon_{\mathrm{eff}}(\boldsymbol{r})$. In summary, the spatial distribution of X can expressed as

$$\mathrm{X}(\boldsymbol{r}) \approx -\frac{1}{8}\sum_i \frac{\nabla\rho_i(\boldsymbol{r})\cdot\nabla\rho_i(\boldsymbol{r})}{\rho_i(\boldsymbol{r})} + \frac{1}{4}\nabla^2\rho(\boldsymbol{r}) - \upsilon_{\mathrm{eff}}(\boldsymbol{r})\rho(\boldsymbol{r}) \tag{9}$$

Note that the integral of this KS approximation to $X(\boldsymbol{r})$ over all space equals the total energy of all occupied KS orbitals.[53] Equation 9 expresses this quantity in terms of densities and potentials that can be provided by most quantum mechanics simulation software. A procedure for performing the analysis using BAND[61] is provided in the Supporting Information.

Defining Atoms inside Crystals. With a workable expression for the electron energy density in hand, we can use it to partition materials into atomic fragments, or basins Ω_{A}.[1] Atomic basins Ω_{A} are here defined from three-dimensional seams at which $\nabla X(\boldsymbol{r}) \cdot \boldsymbol{n}(\boldsymbol{r}) = 0$,[1] where $\nabla X(\boldsymbol{r})$ is the gradient of the electron energy density and where $\boldsymbol{n}(\boldsymbol{r})$ is the unit vector normal to the surface at $\boldsymbol{r}$. Our procedure technically mirrors that of QTAIM, where the condition for defining a basin is instead $\nabla\rho(\boldsymbol{r}) \cdot \boldsymbol{n}(\boldsymbol{r}) = 0$.[7,62,63] As we have illustrated in our previous work focused on molecules,[1] and as we shall see, the resulting atomic basins derived from $X(\boldsymbol{r})$ and $\rho(\boldsymbol{r})$ are notably different. We will refer to electron energy basins, Ω_{A}, to distinguish our partitioning approach from QTAIM. We emphasize that there are many ways one can cut a pie, and the topological method described herein is but one possible method for partitioning $X(\boldsymbol{r})$ that we have begun to explore.

Electron energy-derived basins allow for the subsequent calculation of the atomic properties inside materials. For example, the electron energy X_{A} attributed to an atom can be evaluated by integrating $X(\boldsymbol{r})$ over the basins Ω_{A}. In what follows, we will use this electron energy-based definition of atoms inside materials to study three atomic (or ionic) properties: volumes V_{A}, partial charge q_{A} and what we call *in situ* electronegativity, $\overline{\chi}_A^{\mathrm{val}}$.[1]

Computational Details. All DFT calculations were made using the exchange-correlation functionals PBE[59,60] in combination with triple-ζ polarized basis sets as implemented in BAND 2019.[61] BAND has recently been developed to support direct output of $X(\boldsymbol{r})$, as approximated by eq 9 (see the Supporting Information). Isolated atoms used as references in the evaluation of *in situ* electronegativity are calculated at the same level of theory and embedded in unit cells of size 8 × 8 × 8 Å for Li, C, N, O and F, and 10 × 10 × 10 Å for K and Ga. For atoms, X can be straightforwardly calculated from eq 2 in terms of the total density of states referenced to vacuum, as explained in ref 34. For calculations of crystalline systems, lattice parameters have been set to equal experimental data (see Supporting Information), while all atomic coordinates have been optimized.[64−67] The open-source code Critic2 was used to perform topological analyses.[63] The error in the number of electrons per each unit cell obtained by integrating the electron density over the electron energy basins, Ω_{A}, with the Yu and Trinkle method,[68] is small: LiF = 0.021% (0.002 e), GaN = 0.009% (0.0035 e), K = 0.019% (0.0037 e), and urea = 0.001% (0.0003 e). A detailed procedure for the evaluation of $X(\boldsymbol{r})$ using BAND is provided in the Supporting Information. Details of how the electronegativity of isolated ions is calculated from experimental data are disclosed in the Supporting Information.

RESULTS AND DISCUSSION

To evaluate our methodology[1] in periodic systems, we look at a selection of metallic, ionic, semiconducting, and molecular crystals (Figure 1).

https://doi.org/10.1021/acs.jpcc.3c07677
J. Phys. Chem. C 2024, 128, 4009−4017

The BCC phase of K is an archetypical simple metal with good thermal and electric conductivities and high reactivity. The FCC phase of LiF is a wide band gap (ca. 14 eV) insulator composed of atoms on the opposite extremes of the electronegativity scale.[30] GaN is probably the most heavily investigated of all the III−V nitride semiconductors.[69−71] The wurtzite ($P6_3mc$) phase of GaN is a very hard material with a band gap of 3.4 eV.[70] Finally, urea is a common molecular case study in crystallography. This material consists of high-quality noncentrosymmetric tetragonal $P\bar{4}2_1m$ crystals with two molecules per unit cell[72] and its charge density has been carefully studied using synchrotron X-ray[73] and neutron diffraction.[74] Urea is a good example when studying a range of interactions, including strong covalent bonds and weaker intermolecular hydrogen bonds. Our selection of materials is not meant to be exhaustive but acts as proof-of-concept for our methods' utility in distinguishing between different electronic structures in the condensed phase.

Atomic and Ionic Volumes. We look first at the sizes of atoms (and ions) inside our collection of materials. Defining atomic boundaries in open (e.g., molecular) systems is not trivial, but can, for instance, be done successfully using different cutoff criteria. The electron density[75,76] and properties of valence orbitals are some of the possibilities.[36,77−79] For crystals, there exist other options.[76,80−83] We here choose to attribute atomic volumes V_A directly to the volume of electron energy basins Ω_A. This choice is possible because the gradient field of the electron energy density exclusively separates space into nuclear-centered basins.

In Table 1, volumes of electron energy basins are compared with conventional QTAIM basins (i.e., those derived from $\rho(\boldsymbol{r})$) and with van der Waals volumes of spherical nonbonded atoms in vacuum calculated from a 0.001 e bohr^{-3} electron density cutoff criteria.[76]

Table 1. Atomic (or Ionic) Volumes Derived from Topological Analysis of $X(\boldsymbol{r})$, V_A, and from $\rho(\boldsymbol{r})$, V_{QTAIM}, and van der Waals Volumes of Isolated Atoms in Gas Phase, V_{vdW}[a]

system	V_A	V_{QTAIM}	V_{vdW}[d]
K	71.32	71.32	53.7
LiF	4.64	2.88	44.6
LiF	11.68	13.44	18.1
GaN	11.25	9.71	53.0
GaN	11.80	13.34	24.0
$CO(NH_2)_2$	5.96	5.45	28.7
$CO(NH_2)_2$	15.28	18.17	20.9
$CO(NH_2)_2$	15.62	17.85	24.0
$CO(NH_2)_2$[b]	5.08	3.21	18.1
$CO(NH_2)_2$[c]	5.19	3.63	18.1

[a]All volumes are provided in Å^3. [b]Closer to oxygen. [c]further from oxygen. [d]Data from ref 76.

Table 1 reveals expected trends, with atomic sizes varying with formal charges (we quantify atomic charge in the next section). Atoms that we anticipate to be positive in a compound are smaller, while those that are negative are larger. Ionically or covalently bonded atoms also shrink noticeably compared to their nonbonded (V_{VdW}) references. Potassium may appear to stand out in Table 1, as the only atom that expands relative to its vdW-like gas-phase reference. However, this perceived expansion is only a consequence of our choice of vdW reference, which refers to the volume of a spherical nonbonded atom in a vacuum. A body-centered cubic phase packing of nonoverlapping hard spheres makes up ∼68% of the total volume of a crystal, or 53.7 Å^3, which is the V_{vdW} value we list for K. The total per atom volume of such an ideal packing of nonbonded K atoms would be 79 Å^3, which is larger than the per atom volume of the real solid, calculated to be 71.3 Å^3. In other words, and as expected, chemical bonding reduces the volume of elemental K.

We remind that atoms defined from topological analysis of materials are not spherical or overlapping.[81,84] Figure 2 illustrates how, for example, electron energy basins as well as QTAIM basins of Li and F inside LiF appear more cubic and multifaceted than spherical, respectively.

A feature of our method (also apparent in molecules[1]) is that it often—not always—portrays chemical bonds as less polar or ionic compared to QTAIM. Polarity is reflected in terms of atomic size in Table 1, where bonded electron energy basins are consistently more alike, compared to QTAIM. Noticeably, GaN is predicted to consist of atoms of nearly identical dimensions. The formally reduced atoms in urea (O and N) are also calculated as similar in size. To explain why, we look next to quantifications of the number of electrons in each electron energy basin: the partial charges of the bonded atoms.

Atomic Charge. We evaluate atomic partial charges by integrating the electron density over each electron energy basin

$$q_A = Z_A - \int_{\Omega_A} \rho(\boldsymbol{r})\mathrm{d}\boldsymbol{r} \tag{10}$$

where Z_A is the nuclear charge of atom A.

Table 2 exemplifies how X-based atomic charges q_A compare to QTAIM charges, which are derived from the topological analysis of $\rho(\boldsymbol{r})$ instead of $X(\boldsymbol{r})$. In general, and as previously noted,[1] electron energy-derived basins are attributed to partial charges that are less ionic relative to what is predicted by QTAIM. That QTAIM sometimes predicts charges that are high compared to chemical expectations is known and has for instance been discussed by Fonseca Guerra et al.[9]

Our approach for computing partial charge is well in line with chemical expectations: LiF computes as ionic, and the bonds inside urea between C and heteroatoms appear as polar covalent. At the same time, the latter example of organic chemistry is portrayed as markedly less ionic compared to that of QTAIM. In fact, the charges on all atoms in urea are predicted to be smaller in magnitude with our method, and N atoms are particularly affected by the difference in topological analysis. The partial charge predicted for hydrogen atoms q_H is strikingly (∼50%) different compared to QTAIM. For urea, we also provide atomic partial charges inside the isolated molecule (Table 2). Even though differences in absolute values between the $X(\boldsymbol{r})$- and $\rho(\boldsymbol{r})$-based analyses are evident, relative changes when moving from molecule to crystal are similar. Both methods agree that the introduction of intermolecular interactions in the crystalline state is associated with a slight reduction (an increased negative charge) of the O and N atoms and a partial further oxidation of the hydrogen atoms. Our analysis of urea are in line with Spackman et al.[85] who have used multipolar refinement of experimental electron densities to show how the formation of intermolecular interactions and other electrostatic contributions can greatly affect the molecular dipole moments in a crystalline environment.[86]

https://doi.org/10.1021/acs.jpcc.3c07677
J. Phys. Chem. C 2024, 128, 4009−4017

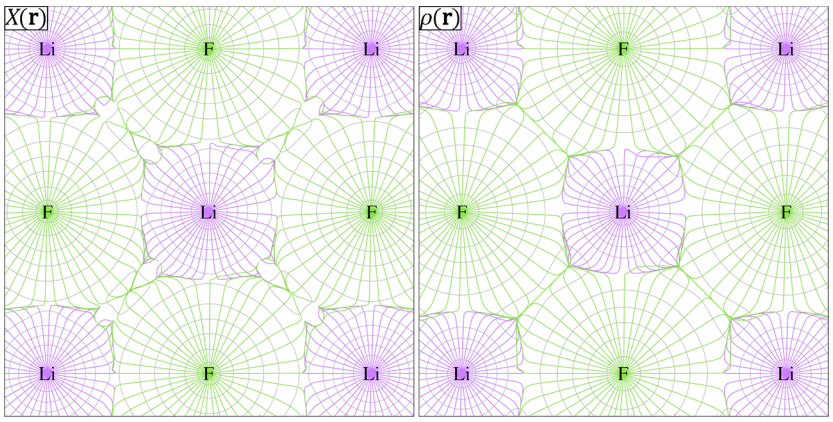

Figure 2. Atomic (ionic) basins in LiF derived from a topological analysis of electron energy density X(r) (left panel) and electron density $\rho(r)$ (right panel).

Table 2. Atomic Partial Charges Derived from the Electron Energy Density, q_A, and from QTAIM[a]

system	q_A	QTAIM
LiF	0.78	0.90
GaN	1.14	1.59
$CO(NH_2)_2$	1.27 (1.26)	1.59 (1.59)
$CO(NH_2)_2$	−0.91(−0.83)	−1.18 (−1.10)
$CO(NH_2)_2$	−0.62 (−0.57)	−1.06 (−1.01)
$CO(NH_2)_2$[b]	0.24 (0.20)	0.45 (0.39)
$CO(NH_2)_2$[c]	0.20 (0.16)	0.41 (0.37)

[a]For urea, atomic charges are provided both for the crystal and for the isolated (C_2 point group) molecule in parentheses. [b]Closer to oxygen. [c]Further from oxygen.

GaN is an example where our methodology helps to provide a different perspective. Our computed partial charges predict a polarity near to $Ga^{1+}N^{-1}$. In contrast, theoretical analysis based on QTAIM describes Ga−N interactions closer to $Ga^{2+}N^{-2}$ (Table 2).[87] We remind that whereas partial charges may be expected to correlate with the magnitude of formal oxidation states, the latter notion is outside our scope and can be quantified by other means (see e.g., 88, 89).

Atomic Electronegativities. Our *in situ* electronegativity, $\overline{\chi}_A^{val}$, is an estimation of the ability of an atom or ion inside a material to hold onto electrons. As also detailed in our previous work,[1] we evaluate *in situ* electronegativity as

$$\overline{\chi}_A^{val} = \overline{\chi}_A^0 + \Delta\overline{\chi}_A \tag{11}$$

where $\overline{\chi}_A^0$ is a reference value from a conventional scale of electronegativity of isolated atoms, quantified experimentally as the average binding energy of valence electrons,[30] and where $\Delta\overline{\chi}_A$ is the quantum mechanically calculated difference between the (all electron) average electron energy of a basin in a molecule $\overline{\chi}_A$ and an atom in isolation, $\overline{\chi}_{A(vac)}$,

$$\Delta\overline{\chi}_A = \overline{\chi}_A - \overline{\chi}_{A(vac)} \tag{12}$$

The average electron energy of a basin is, in turn, evaluated as

$$\overline{\chi}_A = \frac{\int_{\Omega_A} X(\boldsymbol{r})\mathrm{d}\boldsymbol{r}}{\int_{\Omega_A} \rho(\boldsymbol{r})\mathrm{d}\boldsymbol{r}} = \frac{X_A}{n_A} \tag{13}$$

where n_A is the number of electrons attributed to the basin Ω_A. Our set of definitions, eqs 11−13, is a practical choice: because electronegativity is intrinsically linked to valence electrons we effectively normalize the variation of the average electron energy, $\Delta\overline{\chi}_A$ (calculated for all electrons) with an established valence-based scale of electronegativity. This approach for evaluating $\overline{\chi}_A^{val}$ has proven useful both for analyzing chemical bonding and as a potent predictor of pK_a.[1,36] Note that with eq 12 we have introduced empirical parameters, which are experimental but that could be computed.[30] This approach does not reveal how movements of different groups of electronic levels affect the computed $\Delta\overline{\chi}_A$. We aim to return in future work to study the partitioning of $\Delta\overline{\chi}_A$ into valence and core contributions, which is not practical in the current implementation.

To better understand the chemical information provided by *in situ* electronegativity, we look in Table 3 at how this quantity changes when comparing atoms (i.e., electron energy basins, Ω_A) inside crystals with those same atoms in isolation. For the case of urea, we additionally compare the *in situ* electronegativity of atoms inside crystals and in isolated molecules. In Table 3, we also include something uncommon: the electronegativity of selected free ions. These values of average valence electron binding energies of ions in isolation have been derived from experimental electron affinities, ionization potentials, and excitation energies, following the methodology outlined for atoms in reference 30 (see also the Supporting Information). We will make use of these properties of free ions as additional references when interpreting the *in situ* electronegativity calculated for electron energy basins inside crystals.

The formation of a potassium crystal from isolated atoms is characterized by an increase in *in situ* electronegativity, i.e., $\Delta\overline{\chi}_K^{val} > 0$. We remind that a positive $\Delta\overline{\chi}_A^{val}$ for a transformation means that electrons in basin A are on average stabilized. The stabilization, or increase in electronegativity, upon forming solid K from atoms is relatively small, only 1.1 $eV{\cdot}e^{-1}$. In comparison, the formation of H_2 from isolated atoms corresponds to an $\Delta\overline{\chi}$ of 1.828 $eV{\cdot}e^{-1}$.[35] The absolute value of $\overline{\chi}_K^{val}$ is comparatively small in both the atom and the solid and is correctly, and as expected, indicating that the valence electrons in this material are weakly bound. This first example is important because it highlights that electronegativity reflects aspects of the electronic structure even in the absence of net charge transfer between atoms. In the crystallization of potassium, the number of electrons per atom, i.e., the atomic

https://doi.org/10.1021/acs.jpcc.3c07677
J. Phys. Chem. C 2024, 128, 4009−4017

Table 3. Electronegativity of Isolated Atoms and Singly Charged Ions Alongside Estimates for Electron Energy Basins inside (*in situ*) Crystals[a]

system	isolated atom (exp.)[30]	isolated ion (exp.)[b]	basin in crystal (theory)[d]	$\Delta\overline{\chi}_A^{val}$ (theory)
K	4.3	35.7	5.4	1.1
LiF	5.4	75.6	20.6	15.2
LiF	23.3	9.9	15.2	−8.1
GaN	9.9	20.5	47.4	37.5
GaN	16.9	5.1	3.0	−13.9
$CO(NH_2)_2$	13.9	28.7	41.5 (40.2)	27.6 (26.3)
$CO(NH_2)_2$	18.6	5.9	4.9 (4.3)	−13.7 (−14.3)
$CO(NH_2)_2$	16.9	5.1	9.8 (9.6)	−7.0 (−7.3)
$CO(NH_2)_2$[e]	13.6	[c]	14.9 (14.4)	1.3 (0.9)
$CO(NH_2)_2$[f]	13.6	[c]	14.9 (14.5)	1.3 (0.8)

[a] *in situ* electronegativities are also shown for atoms inside an isolated molecule of urea (point group C_2) within parentheses. $\Delta\overline{\chi}_A^{val}$ is the computed difference in electronegativity between bonded atoms inside materials and the isolated atoms. All data are provided in units of eV e^{-1}. [b] The electronegativity for the ground state ($T \rightarrow 0$ K) atomic ions K^+, Li^+, F^-, Ga^+, N^-, C^+, and O^- are derived using data from the NIST Atomic Spectra Database,[90] following the methodology outlined in ref 30. Corresponding valence energy levels are shown in Table S1. [c] H^+ does not have an electronegativity, per definition. The electronegativity for H^-, which is not directly relevant for our discussion, is 0.754 eV e^{-1} (it equals the electron affinity of H). [d] Calculated using eqs 11−13. [e] H closer to oxygen. [f] H further from oxygen.

charge, does not change, yet the electronegativity does. The enhanced electronegativity is the result of a small orbital stabilization brought about by chemical bonding in the material.

Due to the ease of misunderstanding in what follows, we remind readers that electronegativity of atoms can be defined in many ways. It is crucial to understand that electronegativity as we define it need not equalize upon bond formation. The idea of electronegativity equalization, a viewpoint popularized by Sanderson and others,[91−93] posits that atoms that bond each other assume a uniform value of electronegativity. We refer to reference 31 for a rigorous derivation of relationships between $\overline{\chi}_A^{val}$ and the chemical potential, and the introduction of electronegativity *equilibration*. In essence, it is only the chemical potential of ensembles of atoms inside molecules that equalize upon bond formation, not the electronegativity as we define it. Instead, our view on electronegativity allows atoms to retain different identities inside molecules and materials, in line with arguments by several before us.[6,30,31,94−96]

One conceptual phenomenon that is natural if one accepts a definition of electronegativity as the average (binding) energy of valence electrons is electronegativity inversion. We know to expect electronegativity inversion in the formation of polar bonds[1] and will look first to the formation of LiF as an example.

To see why the electronegativity of atomic Li and F will invert upon the formation of LiF, it helps to recall that the polarity in LiF is closer to Li^+F^- than that of neutral atoms (Table 2). In other words, one can approximately think of Li in LiF as a cation with a [He] configuration. The electrons in the Li basin are fewer in number than the nuclear charges of Li, and therefore difficult to perturb or remove. Conversely, electrons in the F basin of LiF are not as strongly bound as they are in the naked F atom. The *in situ* electronegativities shown in Table 3 reflect this situation well with a Li basin ($Li^{+0.78}$) being considerably more electronegative than $F^{-0.78}$. The *in situ* electronegativities calculated in the crystal are, as expected, in-between our experimental reference values for the free atoms and ions, F−F^-, and Li−Li^+, respectively. The *in situ* electronegativity of F in the crystal is indicative of a ∼ 60% transformation toward F^-, in terms of average electron binding. In contrast, the electrons of bound Li appear only 22% on their way to Li^+. The latter comparison with experiment is likely an underestimation caused by the tendency of KS-DFT to underestimate the binding energies of core levels. Such effects will be especially pronounced in the case of Li → Li^+, as the 1s former core becomes a valence shell.

The same effect of electronegativity inversion is showcased in GaN but with a larger magnitude. Whereas the electronegativities of isolated Ga and N atoms do not differ as much as Li and F, the former pair undergo a more drastic change upon bond formation, eventually differing by 44.4 eV·e^{-1} (Table 3). With our perspective, GaN is composed of highly electronegative Ga, while bound N takes an electronegativity comparable to atomic Cs.[30] We primarily attribute the larger magnitude of the electronegativity inversion to a larger number of formally exchanged electrons (three), compared with that in LiF (one). The *in situ* electronegativity calculated for N is (maybe fortuitously) smaller than our experimental reference value for an isolated N^-, agreeing with this atom carrying more than one negative charge in GaN. Similarly, the *in situ* electronegativity of Ga computes as larger than for isolated Ga^+, consistent with an atomic charge larger than one in GaN. At the same time, we emphasize that the utility of *in situ* electronegativities goes well beyond a secondary description of charge transfer. It provides spatial information on electron binding. Our data in Table 3 predicts that electron detachment from GaN should occur primarily from N valence electrons. This prediction is, for instance, supported by soft-X-ray emission experiments, which show that the top of the valence band of GaN is dominated by N 2p levels.[97]

Whereas trends in changing partial and *in situ* electronegativity often go hand in hand (Tables 2 and 3), the latter quantity does not always change in the way one might immediately expect. Consider for example the formation of crystalline urea from isolated molecules (molecular data is given within parentheses in Table 2). This process is primarily associated with strong intermolecular interactions in the form of hydrogen bonds. Several atoms in this example (H and C) follow the expected trend where oxidation of an element also renders it increasingly electronegative, or reduction less electronegative. However, for O and N the opposite is predicted! While the partial charge of O decreases from −0.83 to −0.91 and that of N from −0.57 to −0.62 (Table 2) upon formation of the urea crystal, the *in situ* electronegativity of these atoms increases. We have made a similar prediction in the case of nucleobase pairing where also H is oxidized while becoming less electronegative.[1] These examples again serve to remind that whereas quantifications of partial charge may be useful for approximating where electrons move, *in situ* electronegativity tells a different story: it reveals how well electrons are bound in different locations.

By taking a MO perspective, we can understand to expect an increased *in situ* electronegativity for elements that partake in hydrogen bonding. In MO theory, a hydrogen bond is primarily an orbital stabilization effect, i.e., an interaction driven by the lowering of electronic energies. In brief, the MO

https://doi.org/10.1021/acs.jpcc.3c07677
J. Phys. Chem. C 2024, 128, 4009−4017

responsible for such an interaction is typically delocalized over all participating atoms (a two-electron-three-center bond over O, N, and H in our example). The *in situ* electronegativity that we quantify is effectively a spatially resolved average MO stabilization (cf., eq 3). As such, our methodological framework allows for a natural conceptual merger between MO theory and quantum chemical topological approaches to electronic structure analysis.

CONCLUSIONS

This work introduces a quantum chemical methodology that allows for the quantification of atomic (or ionic) volumes, partial charges, and electronegativity inside condensed phase materials. This development stems from previous work and theory focused on molecular systems[1] and opens the door for comparing chemical concepts quantified both inside molecules in vacuum, in crystalline solids, and, in principle, following simulations of liquids.

The core idea behind our methodology is to perform topological analysis on the electron energy density, $X(\boldsymbol{r})$, which permits the definition of topological atoms and their respective properties. The electron energy density is defined in eq 1, as a product of the physically observable electron density $\rho(\boldsymbol{r})$ and the average electron energy $\overline{\chi}(\boldsymbol{r})$. The latter quantity can be approximated from the average of occupied MOs. An important extension of our approach is to allow for the study of extended systems by expressing $X(\boldsymbol{r})$ not in terms of KS average orbitals but as a sum of energy densities.

We attribute the valence electron part of $\overline{\chi}(\boldsymbol{r})$ to electronegativity and show how this concept can be quantified for regions of space associated with atoms inside materials (molecules and crystals). Discussions on electronegativity inversion upon bond formation are argued to be a natural consequence of our choice of definition for this descriptor. To aid our discussion of the properties of atoms inside crystals, we introduce experimentally determined electronegativities of some isolated ions: H^-, Li^+, C^+, N^-, O^-, F^-, K^+, and Ga^+. We refer to previous work for a more in-depth analysis and discussion of electronegativity as the average electron energy in general[30] and its relation to the chemical potential.[31] We consider the development presented herein important for demonstrating the potential benefits of combining the sometimes historically disparate approaches to quantum chemical topology and MO theory.

ASSOCIATED CONTENT

Supporting Information

The Supporting Information is available free of charge at https://pubs.acs.org/doi/10.1021/acs.jpcc.3c07677.

Additional details on the methodology, theoretical background and supporting data, including cif-files of all considered crystal structures (PDF)

Crystallographic data of all considered crystal structures (ZIP)

AUTHOR INFORMATION

Corresponding Author

Martin Rahm − *Department of Chemistry and Chemical Engineering, Chalmers University of Technology, Gothenburg 41258, Sweden;* orcid.org/0000-0001-7645-5923; Email: martin.rahm@chalmers.se

Authors

Stefano Racioppi − *Department of Chemistry and Chemical Engineering, Chalmers University of Technology, Gothenburg 41258, Sweden;* orcid.org/0000-0002-4174-1732

Per Hyldgaard − *Department of Microtechnology and Nanoscience—MC2, Chalmers University of Technology, Gothenburg 41258, Sweden;* orcid.org/0000-0001-5810-8119

Complete contact information is available at: https://pubs.acs.org/10.1021/acs.jpcc.3c07677

Author Contributions

Conceptualization: M.R.; Methodology and Investigation: S.R., M.R., P.H.; Writing−original draft: M.R., S.R. The manuscript was written through contributions of all authors. All authors have given approval to the final version of the manuscript.

Funding

Chalmers University of Technology (M.R.) The Carl Trygger Foundation grant 19:294 (M.R.) The Swedish Foundation for Strategic Research contract IMF17-0324 (P.H.). Sweden's innovation agency Vinnova, through Project No. 2020-05179 (P.H.) This research relied on computational resources provided by the Swedish National Infrastructure for Computing (SNIC) at C3SE, NSC and PDC partially funded by the Swedish Research Council through grant agreement no. 2018-05973, and by the National Academic Infrastructure for Supercomputing in Sweden (NAISS) at C3SE and NSC partially funded by the Swedish research council through grant agreement no. 2022-06725. One of our allocations were SNIC2022-3-16 (PH).

Notes

The authors declare no competing financial interest.

ACKNOWLEDGMENTS

We acknowledge financial support from Chalmers University of Technology and the Carl Trygger Foundation (grant 19:294). We thank Alberto Otero-De-La-Roza for his help in providing a version of Critic2 that can analyze output generated with BAND.

REFERENCES

(1) Racioppi, S.; Rahm, M. *in situ* Electronegativity and the Bridging of Chemical Bonding Concepts. *Chem. − Eur. J.* **2021**, *27* (72), 18156−18167.

(2) Gonthier, J. F.; Steinmann, S. N.; Wodrich, M. D.; Corminboeuf, C. Quantification of "Fuzzy" Chemical Concepts: A Computational Perspective. *Chem. Soc. Rev.* **2012**, *41* (13), 4671−4687.

(3) Szarek, P.; Grochala, W. Most Probable Distance between the Nucleus and HOMO Electron: The Latent Meaning of Atomic Radius from the Product of Chemical Hardness and Polarizability. *J. Phys. Chem. A* **2014**, *118* (44), 10281−10287.

(4) Szarek, P.; Chlebicki, A.; Grochala, W. Atomic/Ionic Radius as Mathematical Limit of System Energy Evolution. *J. Phys. Chem. A* **2019**, *123* (3), 682−692.

(5) Batsanov, S. S. Energy Electronegativity and Chemical Bonding. *Molecules* **2022**, *27* (23), 8215.

(6) Politzer, P.; Murray, J. S. Electronegativity: A Continuing Enigma. *J. Phys. Org. Chem.* **2023**, *36*, No. e4406.

(7) Bader, R. F. W. *Atoms in Molecules: A Quantum Theory, International Series of Monographs on Chemistry*; Oxford Science Publications: Oxford, 1990; Vol. *22*.

(8) Hirshfeld, F. L. Bonded-Atom Fragments for Describing Molecular Charge Densities. *Theor. Chim. Acta* **1977**, *44* (2), 129−138.

(9) Fonseca Guerra, C.; Handgraaf, J. W.; Baerends, E. J.; Bickelhaupt, F. M. Voronoi Deformation Density (VDD) Charges: Assessment of the Mulliken, Bader, Hirshfeld, Weinhold, and VDD Methods for Charge Analysis. *J. Comput. Chem.* **2004**, *25* (2), 189−210.
(10) Nelson, R.; Ertural, C.; George, J.; Deringer, V. L.; Hautier, G.; Dronskowski, R. LOBSTER: Local Orbital Projections, Atomic Charges, and Chemical-Bonding Analysis from Projector-Augmented-Wave-Based Density-Functional Theory. *J. Comput. Chem.* **2020**, *41* (21), 1931−1940.
(11) Batsanov, S. S. Electronegativities of Metal Atoms in Crystalline Solids. *Inorg. Mater.* **2001**, *37* (1), 23−30.
(12) Batsanov, S. S. Metal Electronegativity Calculations from Spectroscopic Data. *Russ. J. Phys. Chem. A* **2005**, *79* (5), 725−731.
(13) Batsanov, S. S. System of Metal Electronegativities Calculated from the Force Constants of the Bonds. *Russ. J. Inorg. Chem.* **2011**, *56* (6), 906−912.
(14) Batsanov, S. S. Calculating Atomic Charges in Molecules and Crystals by a New Electronegativity Equalization Method. *J. Mol. Struct.* **2011**, *1006* (1−3), 223−226.
(15) Luo, Y. R.; Benson, S. W. The Covalent Potential: A Simple and Useful Measure of the Valence-State Electronegativity for Correlating Molecular Energetics. *Acc. Chem. Res.* **1992**, *25* (8), 375−381.
(16) Li, K.; Xue, D. Estimation of Electronegativity Values of Elements in Different Valence States. *J. Phys. Chem. A* **2006**, *110* (39), 11332−11337.
(17) Li, K.; Wang, X.; Xue, D. Electronegativities of Elements in Covalent Crystals. *J. Phys. Chem. A* **2008**, *112* (34), 7894−7897.
(18) Li, K.; Wang, X.; Zhang, F.; Xue, D. Electronegativity Identification of Novel Superhard Materials. *Phys. Rev. Lett.* **2008**, *100*, No. 235504.
(19) Pendás, A. M.; Costales, A.; Luaña, V. Ions in Crystals: The Topology of the Electron Density in Ionic Materials. III. Geometry and Ionic Radii. *J. Phys. Chem. B* **1998**, *102* (36), 6937−6948.
(20) Boyd, R. J.; Edgecombe, K. E. Atomic and Group Electronegativities from the Electron Density Distributions of Molecules. *J. Am. Chem. Soc.* **1988**, *110* (13), 4182−4186.
(21) Boyd, R. J.; Boyd, S. L. Group Electronegativities from the Bond Critical Point Model. *J. Am. Chem. Soc.* **1992**, *114* (5), 1652−1655.
(22) Komorowski, L. Electronegativity through the Energy Function. *Chem. Phys. Lett.* **1983**, *103* (3), 201−204.
(23) Komorowski, L. Electronegativity and Hardness in the Chemical Approximation. *Chem. Phys.* **1987**, *114* (1), 55−71.
(24) Van Genechten, K.; Mortier, W.; Geerlings, P. Framework Electronegativity: A Novel Concept in Solid State Chemistry. *J. Chem. Soc. Chem. Commun.* **1986**, *5063* (16), 1278−1279.
(25) Mortier, W. J.; Ghosh, S. K.; Shankar, S. Electronegativity Equalization Method for the Calculation of Atomic Charges in Molecules. *J. Am. Chem. Soc.* **1986**, *108* (15), 4315−4320.
(26) Tachibana, A. Electronic Energy Density in Chemical Reaction Systems. *J. Chem. Phys.* **2001**, *115* (8), 3497−3518.
(27) Roothaan, C. C. J. New Developments in Molecular Orbital Theory. *Rev. Mod. Phys.* **1951**, *23* (2), 69−89.
(28) Hoffmann, R. A Chemical and Theoretical Way to Look at Bonding on Surfaces. *Rev. Mod. Phys.* **1988**, *60* (3), 601−628.
(29) Albright, T. A.; Burdett, J. K.; Whangbo, M. H. *Orbital Interactions in Chemistry*; Wiley: Chicester, 2013.
(30) Rahm, M.; Zeng, T.; Hoffmann, R. Electronegativity Seen as the Ground State Average Valence Electron Binding Energy. *J. Am. Chem. Soc.* **2019**, *141*, 342−351.
(31) Sessa, F.; Rahm, M. Electronegativity Equilibration. *J. Phys. Chem. A* **2022**, *126* (32), 5472−5482.
(32) Sessler, C. D.; Rahm, M.; Becker, S.; Goldberg, J. M.; Wang, F.; Lippard, S. J. CF2H, a Hydrogen Bond Donor. *J. Am. Chem. Soc.* **2017**, *139* (27), 9325−9332.
(33) Sessa, F.; Olsson, M.; Söderberg, F.; Wang, F.; Rahm, M. Experimental Quantum Chemistry: A Hammett-Inspired Fingerprinting of Substituent Effects. *ChemPhysChem* **2021**, *22* (6), 569−576.
(34) Rahm, M.; Hoffmann, R. Toward an Experimental Quantum Chemistry: Exploring a New Energy Partitioning. *J. Am. Chem. Soc.* **2015**, *137* (32), 10282−10291.
(35) Rahm, M.; Hoffmann, R. Distinguishing Bonds. *J. Am. Chem. Soc.* **2016**, *138* (11), 3731−3744.
(36) Rahm, M.; Cammi, R.; Ashcroft, N. W.; Hoffmann, R. Squeezing All Elements in the Periodic Table: Electron Configuration and Electronegativity of the Atoms under Compression. *J. Am. Chem. Soc.* **2019**, *141*, 10253−10271.
(37) Politzer, P.; Murray, J. S.; Bulat, F. A. Average Local Ionization Energy: A Review. *J. Mol. Model.* **2010**, *16* (11), 1731−1742.
(38) Ryabinkin, I. G.; Staroverov, V. N. Average Local Ionization Energy Generalized to Correlated Wavefunctions. *J. Chem. Phys.* **2014**, *141* (8), No. 084107.
(39) Racioppi, S.; Lolur, P.; Hyldgaard, P.; Rahm, M. A Density Functional Theory for the Average Electron Energy. *J. Chem. Theory Comput.* **2023**, *19*, 799−807.
(40) Sjöberg, P.; Murray, J. S.; Brinck, T.; Politzer, P. Average Local Ionization Energies on the Molecular Surfaces of Aromatic Systems as Guides to Chemical Reactivity. *Can. J. Chem.* **1990**, *68* (8), 1440−1443.
(41) Bulat, F. A.; Levy, M.; Politzer, P. Average Local Ionization Energies in the Hartree-Fock and Kohn-Sham Theories. *J. Phys. Chem. A* **2009**, *113* (7), 1384−1389.
(42) Politzer, P.; Abu-Awwad, F.; Murray, J. S. Comparison of Density Functional and Hartree-Fock Average Local Ionization Energies on Molecular Surfaces. *Int. J. Quantum Chem.* **1998**, *69* (4), 607−613.
(43) Murray, J. S.; Brinck, T.; Politzer, P. Applications of Calculated Local Surface Ionization Energies to Chemical Reactivity. *J. Mol. Struct. THEOCHEM* **1992**, *255*, 271−281.
(44) Politzer, P.; Murray, J. S.; Concha, M. C. The Complementary Roles of Molecular Surface Electrostatic Potentials and Average Local Ionization Energies with Respect to Electrophilic Processes. *Int. J. Quantum Chem.* **2002**, *88*, 19−27.
(45) Bulat, F. A.; Burgess, J. S.; Matis, B. R.; Baldwin, J. W.; MacAveiu, L.; Murray, J. S.; Politzer, P. Hydrogenation and Fluorination of Graphene Models: Analysis via the Average Local Ionization Energy. *J. Phys. Chem. A* **2012**, *116* (33), 8644−8652.
(46) Murray, J. S.; Shields, Z. P. I.; Lane, P.; Macaveiu, L.; Bulat, F. A. The Average Local Ionization Energy as a Tool for Identifying Reactive Sites on Defect-Containing Model Graphene Systems. *J. Mol. Model.* **2013**, *19* (7), 2825−2833.
(47) Murray, J. S.; Brinck, T.; Politzer, P. Surface Local Ionization Energies and Electrostatic Potentials of the Conjugate Bases of a Series of Cyclic Hydrocarbons in Relation to Their Aqueous Acidities. *Int. J. Quantum Chem.* **1991**, *40* (18 S), 91−98.
(48) Politzer, P.; Jin, P.; Murray, J. S. Atomic Polarizability, Volume and Ionization Energy. *J. Chem. Phys.* **2002**, *117* (18), 8197−8202.
(49) Jin, P.; Murray, J. S.; Politzer, P. Local Ionization Energy and Local Polarizability. *Int. J. Quantum Chem.* **2004**, *96* (4), 394−401.
(50) Politzer, P.; Murray, J. S. Electronegativity—a Perspective. *J. Mol. Model.* **2018**, *24* (214), 1−8.
(51) Politzer, P.; Peralta-Inga Shields, Z.; Bulat, F. A.; Murray, J. S. Average Local Ionization Energies as a Route to Intrinsic Atomic Electronegativities. *J. Chem. Theory Comput.* **2011**, *7* (2), 377−384.
(52) Ayers, P. W.; Parr, R. G.; Nagy, A. Local Kinetic Energy and Local Temperature in the Density-Functional Theory of Electronic Structure. *Int. J. Quantum Chem.* **2002**, *90* (1), 309−326.
(53) Parr, R. G.; Yang, W. *Density-Functional Theory of Atoms and Molecules*; Oxford University Press, Ed.: Oxford, 1989.
(54) Tal, Y.; Bader, R. F. W. Studies of the Energy Density Functional Approach. I. Kinetic Energy. *Int. J. Quantum Chem.* **1978**, *14* (12), 153−168.
(55) Anderson, J. S. M.; Ayers, P. W.; Hernandez, J. I. R. How Ambiguous Is the Local Kinetic Energy? *J. Phys. Chem. A* **2010**, *114* (33), 8884−8895.

https://doi.org/10.1021/acs.jpcc.3c07677
J. Phys. Chem. C 2024, 128, 4009−4017

(56) Bader, R. F. W.; Preston, H. J. T. The Kinetic Energy of Molecular Charge Distributions and Molecular Stability. *Int. J. Quantum Chem.* **1969**, *3* (3), 327−347.
(57) Nagy; Parr, R. G.; Liu, S. Local Temperature in an Electronic System. *Phys. Rev. A - At. Mol. Opt. Phys.* **1996**, *53* (5), 3117−3121.
(58) Gal, T.; Nagy, A. Local Temperature in Molecules. *Mol. Phys.* **1997**, *91* (5), 873−880.
(59) Perdew, J. P.; Burke, K.; Ernzerhof, M. Generalized Gradient Approximation Made Simple. *Phys. Rev. Lett.* **1996**, *77* (18), 3865−3868.
(60) Perdew, J. P.; Burke, K.; Ernzerhof, M. [ERRATA] Generalized Gradient Approximation Made Simple. *Phys. Rev. Lett.* **1996**, *77* (18), 3865−3868.
(61) Philipsen, P. H. T.; te Velde, G.; Baerends, E. J.; Berger, J. A.; de Boeij, P. L.; Franchini, M.; Groeneveld, J. A.; Kadantsev, E. S.; Klooster, R.; Kootstra, F.; Pols, M. C. W. M.; Romaniello, P.; Raupach, M.; Skachkov, D. G.; Snijders, J. G.; Verzijl, C. J. O.; Gil, J. A. C.; Thijssen, J. M.; Wiesenekker, G.; Peeples, C. A.; Schreckenbach, G.; Ziegler, T. *BAND 2019.3, SCM, Theoretical Chemistry*; Vrije Universiteit: Amsterdam, The Netherlands, http://www.scm.com.
(62) Biegler-König, F. W.; Tung, T. N.-D.; Tal, Y.; Bader, R. F. W.; Duke, A. J. Calculation of the Average Properties of Atoms in Molecules. *J. Phys. B: At., Mol. Opt. Phys.* **1981**, *14*, 2739−2751.
(63) Otero-De-La-Roza, A.; Johnson, E. R.; Luaña, V. Critic2: A Program for Real-Space Analysis of Quantum Chemical Interactions in Solids. *Comput. Phys. Commun.* **2014**, *185* (3), 1007−1018.
(64) Barrett, C. S. X-Ray Study of the Alkali Metals at Low Temperatures. *Acta Crystallogr.* **1956**, *9* (8), 671−677.
(65) Dupré, K.; Recker, K.; Wallrafen, F. Directional Solidification of the LiF - LiBaF3 Eutectic. *Mater. Res. Bull.* **1992**, *27* (3), 311−318.
(66) Kaminski, M.; Podsiadlo, S.; Wozniak, K.; Dobrzycki, L.; Jakiela, R.; Barcz, A.; Psoda, M.; Mizera, J. Growth and Structural Properties of Thick GaN Layers Obtained by Sublimation Sandwich Method. *J. Cryst. Growth* **2007**, *303* (2), 395−399.
(67) Sklar, N.; Senko, M. E.; Post, B. Thermal Effects in Urea: The Crystal Structure at − 140°C and at Room Temperature. *Acta Crystallogr.* **1961**, *14* (7), 716−720.
(68) Yu, M.; Trinkle, D. R. Accurate and Efficient Algorithm for Bader Charge Integration. *J. Chem. Phys.* **2011**, *134*, No. 064111.
(69) Vurgaftman, I.; Meyer, J. R. Band Parameters for Nitrogen-Containing Semiconductors. *J. Appl. Phys.* **2003**, *94* (6), 3675−3696.
(70) Strite, S.; Morkoc, H. GaN, AlN, and InN: A Review. *J. Vac. Sci. Technol. B Microelectron. Nanom. Struct.* **1992**, *10*, 1237−1266.
(71) Jain, S. C.; Willander, M.; Narayan, J.; Van Overstraeten, R. III−Nitrides: Growth, Characterization, and Properties. *J. Appl. Phys.* **2000**, *87* (3), 965−1006.
(72) Vaughan, P.; Donohue, J. The Structure of Urea. Interatomic Distances and Resonance in Urea and Related Compounds. *Acta Crystallogr.* **1952**, *5* (4), 530−535.
(73) Birkedal, H.; Madsen, D.; Mathiesen, R. H.; Knudsen, K.; Weber, H. P.; Pattison, P.; Schwarzenbach, D. The Charge Density of Urea from Synchrotron Diffraction Data. *Acta Crystallogr. Sect. A Found. Crystallogr.* **2004**, *60* (5), 371−381.
(74) Swaminathan, S.; Craven, B. M.; McMullan, R. K. The Crystal Structure and Molecular Thermal Motion of Urea at 12, 60 and 123 K from Neutron Diffraction. *Acta Crystallogr. Sect. B* **1984**, *40* (3), 300−306.
(75) Boyd, R. J. The Relative Sizes of Atoms. *J. Phys. B At. Mol. Phys.* **1977**, *10* (12), 2283−2291.
(76) Rahm, M.; Hoffmann, R.; Ashcroft, N. W. Atomic and Ionic Radii of Elements 1−96. *Chem. - A Eur. J.* **2016**, *22* (41), 14625−14632.
(77) Slater, J. C. Atomic Shielding Constants. *Phys. Rev.* **1930**, *36* (1), 57−64.
(78) Clementi, E.; Raimondi, D. L.; Reinhardt, W. P. Atomic Screening Constants from SCF Functions. II. Atoms with 37 to 86 Electrons. *J. Chem. Phys.* **1967**, *47* (4), 1300−1307.
(79) Waber, J. T.; Cromer, D. T. Orbital Radii of Atoms and Ions. *J. Chem. Phys.* **1965**, *42* (12), 4116−4123.
(80) Bondi, A. Van Der Waals Volumes and Radii. *J. Phys. Chem.* **1964**, *68* (3), 441−451.
(81) Bader, R. F. W.; Carroll, M. T.; Cheeseman, J. R.; Chang, C. Properties of Atoms in Molecules: Atomic Volumes. *J. Am. Chem. Soc.* **1987**, *109* (26), 7968−7979.
(82) Tschauner, O. An Observation Related to the Pressure Dependence of Ionic Radii. *geosciences* **2022**, *12* (6), 246.
(83) Mroz, A. M.; Davenport, A. M.; Sterling, J.; Davis, J.; Hendon, C. H. An Electric Field-Based Approach for Quantifying Effective Volumes and Radii of Chemically Affected Space. *Chem. Sci.* **2022**, *13* (22), 6558−6566.
(84) Bader, R. F. W.; Austen, M. A. Properties of Atoms in Molecules: Atoms under Pressure. *J. Chem. Phys.* **1997**, *107* (11), 4271−4285.
(85) Spackman, M. A.; Byrom, P. G.; Alfredsson, M.; Hermansson, K. Influence of Intermolecular Interactions on Multipole-Refined Electron Densities. *Acta Crystallogr. Sect. A Found. Crystallogr.* **1999**, *55* (1), 30−47.
(86) Spackman, M. A.; Munshi, P.; Jayatilaka, D. The Use of Dipole Lattice Sums to Estimate Electric Fields and Dipole Moment Enhancement in Molecular Crystals. *Chem. Phys. Lett.* **2007**, *443* (1−3), 87−91.
(87) Costales, A.; Blanco, M. A.; Martín Pendás, Á.; Kandalam, A. K.; Pandey, R. Chemical Bonding in Group III Nitrides. *J. Am. Chem. Soc.* **2002**, *124* (15), 4116−4123.
(88) Ramos-Cordoba, E.; Postils, V.; Salvador, P. Oxidation States from Wave Function Analysis. *J. Chem. Theory Comput.* **2015**, *11* (4), 1501−1508.
(89) Walsh, A.; Sokol, A. A.; Buckeridge, J.; Scanlon, D. O.; Catlow, C. R. A. Oxidation States and Ionicity. *Nat. Mater.* **2018**, *17* (11), 958−964.
(90) Kramida, A.; Ralchenko, Y.; Reader, J.; Salomon, E. B.; Olsen, K.; Eric, C.; Carpentier, T.; Zimmerman, A.; Hamins-Puertolas, A.; Hamins-Puertolas, M.; Sharova, A.; Tan, G. *NIST Atomic Spectra Database (Ver. 5.11), [Online]*; National Institute of Standards and Technology: Gaithersburg, MD, 2024. Available: Https://Physics.Nist.Gov/Asd, 2024, January 28.
(91) Sanderson, R. T. An Interpretation of Bond Lengths and a Classification of Bonds. *Science (80-.)* **1951**, *114* (2973), 670−672.
(92) Sanderson, R. T. Partial Charges on Atoms in Organic Compounds. *Science (80-.)* **1955**, *121* (3137), 207−208.
(93) Parr, R. G.; Donnelly, R. A.; Levy, M.; Palke, W. E. Electronegativity: The Density Functional Viewpoint. *J. Chem. Phys.* **1978**, *68* (8), 3801−3807.
(94) Allen, L. C. Electronegativity Is the Average One-Electron Energy of the Valence-Shell Electrons in Ground-State Free Atoms. *J. Am. Chem. Soc.* **1989**, *111* (25), 9003−9014.
(95) Bergmann, D.; Hinze, J. Electronegativity and Molecular Properties. *Angew. Chemie (International Ed. English)* **1996**, *35* (2), 150−163.
(96) Hinze, J. The Concept of Electronegativity of Atoms in Molecules. *Theor. Comput. Chem.* **1999**, *6*, 189−212.
(97) Stagarescu, C.; Duda, L. C.; Smith, K.; Guo, J.; Nordgren, J. Electronic Structure of GaN Measured Using Soft-x-Ray Emission and Absorption. *Phys. Rev. B: Condens. Matter Mater. Phys.* **1996**, *54* (24), R17335−R17338.

https://doi.org/10.1021/acs.jpcc.3c07677
J. Phys. Chem. C 2024, 128, 4009−4017